PARAMETER IDENTIFICATION VIA KALMAN FILTER ON A MODEL MOTOR GLIDER

M. Strauss*†

Abstract

This work aims to improve the flight dynamic model of the model aircraft Vitesse V2 through parameter identification using an extended and unscented Kalman filter (EKF and UKF). A flight mechanical model is integrated into the filter algorithms in MATLAB to estimate the aircraft's states and aerodynamic coefficients. Two variants of the UKF are examined: a general case with nonlinear noise and a simplified case assuming additive zero-mean noise. By conducting flight tests, data is obtained to optimize the filter design parameters as well as for the actual parameter identification.

The results show that the simplified UKF provides the best balance between capturing system dynamics and ensuring parameter convergence. Its superior performance over the EKF is likely due to the sigma point method, which enhances the accuracy of state and parameter estimates. Focusing on aerodynamic parameter estimation and using longer datasets significantly improves accuracy and convergence of the estimated parameters.

Keywords Aerodynamic Parameter Identification, Extended Kalman Filter, Unscented Kalman Filter

NOMENC	LATURE		p,q,r	roll, pitch, yaw rate	$\mathrm{rad/s}$
Symbols			Q	system noise covariance	
α	angle of attack	\deg	R	measurement noise covariance	
α_{UKF}	scaling parameters for UKF		\underline{R}_b^A	aerodyn. force vector, body frame	N
β	side slip	deg	σ_{rel}	relative standard deviation	
β_{UKF}	scaling parameters for UKF		\underline{T}_b	thrust vector, body frame	N
<u>d</u>	disturbances		$\underline{\Theta}$	parameters to estimate	
$-\delta_t$	thrust throttle level		\underline{u}	control inputs	
h	altitude	m	$u_{k_b}, v_{k_b}, w_{k_b}$	translational velocities along the x,y,z axes	m/s
K	Kalman gain		\underline{v}	measurement noise	
κ	scaling parameters for UKF		\underline{V}_{k_b}	path fixed velocity in body frame	m/s
\underline{M}_{CG}^{A}	aerodyn moment at CG	Nm	\underline{V}_w	Wind velocity	$\mathrm{m/s}$
\underline{M}_{CG}^T	thrust moment at CG	Nm	\underline{w}	process noise	
<u>ω</u>	aileron control surface deflection/s	rad	\underline{W}_b	Weight force vector, body frame	N
— Р	estimation error covariance matrix		\underline{x}	states	
		,	\underline{x}_a	augmented states	
P_a	estimation error of the augmented sy covariance matrix	stem	\underline{y}	outputs	
p_{dyn}	dynamic pressure	Pa	<u>z</u>	measured outputs	
Φ,Θ,Ψ	Euler angles	rad	ζ,η,ξ	rudder, elevator, aileron deflection	\deg

^{*} Technical University of Berlin, Department of Flight Mechanics, Flight Control, and Aeroelasiticity, Berlin, Germany

 $^{^\}dagger$ Fraunhofer Institute for Physical Measurement Techniques IPM, Freiburg, Germany



FIG 1. Vitesse V2 model glider [1]

Abbreviations

AC Aircraft

CG center of gravity

EKF Extended Kalman Filter

KF Kalman Filter

NMSE Normalized Mean Squared Error

PWM Pulse Width Modulated

UKF Unscented Kalman Filter

1. INTRODUCTION

Accurate physical models are essential for simulating systems under varying conditions and for developing control algorithms, with complexity depending on the application. This work aims to improve the model of the Vitesse V2 motor glider by estimating aerodynamic parameters and system states using different types of Kalman filters. Implementing these filters on the flight computer enables state feedback control, adaptive control, and real-time model verification, which can benefit not only this research aircraft but potentially other types as well. The objective of this work therefore focuses on an identification problem (finding the system behavior based on known inputs and outputs). This involves using a phenomenological model, which is based on equations of motion and provides traceable internal behavior. values are used as initial estimates for the parameters that will be improved using actual flight test data that is collected during a test campaign conducted in the course of this work. Subsequently the log data of those flight tests is used for the recursive parameter estimation using different Kalman Filters.

The Kalman Filter (KF), introduced by Rudolf Kalman in 1961 [2], estimates state variables based on system inputs, outputs, and a linear model. The Extended Kalman Filter (EKF) was later developed to handle nonlinear systems by linearizing them around each state, allowing it to be used for both state and parameter estimation [3]. Various KF variants have since emerged, including the adaptive ROSE-Filter (Rapid Ongoing Stochastic covariance Estimation-Filter) described in [4] and the Unscented Kalman Filter (UKF) [3,5], which improves upon the EKF by avoiding errors in linear propagation through the sigma point method. The UKF is widely used

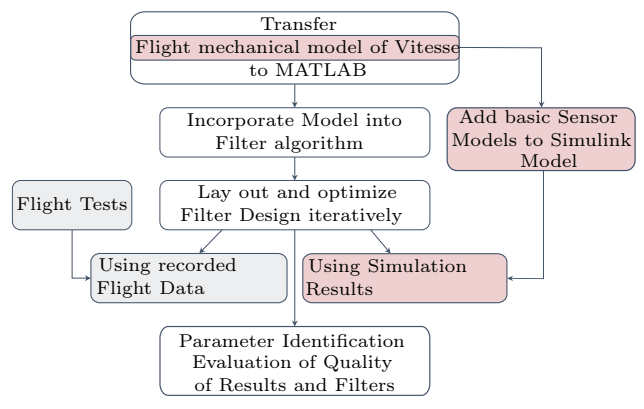


FIG 2. Procedure

in fields like aerospace, navigation, and robotics, and remains an active area of research.

To achieve parameter estimation using different types of Kalman filters, the existing flight mechanical model of the Vitesse V2 is transferred from Simulink to MAT-LAB. This model is integrated into the EKF and UKF algorithms, with the filter design optimized using both simulated sensor data and real flight test data. The flight tests are prepared and conducted and subsequently provide the log data that are then used for the final parameter identification and the evaluation of the filter performance as described in figure 2.

2. FLIGHT MECHANICAL MODEL

The mathematical model of the aircraft (AC) and its flight dynamics is needed to simulate the AC together with the Kalman Filter. However, it is also part of the filtering algorithm itself as the Kalman filter is an optimal state observer [6].

The basic structure of the flight mechanical model shown in figure 3 is based on Newton's 2nd law. A more detailed derivation can be found in [7].

The states vector that is part of the representation of the model results from the derivation of the equations of motion. By including the path velocity in the body frame \underline{V}_{k_b} , the angular rates $\underline{\omega}$, the Euler angles Φ , Θ and Ψ and the height h it is defined in a way that is common practice to sufficiently describe the behavior of the AC.

$$\underline{x} = \begin{bmatrix} \underline{V}_{k_b} \\ \underline{\omega} \\ \begin{bmatrix} \Phi & \Theta & \Psi \end{bmatrix}^T \end{bmatrix}$$

The control variable vector \underline{u} is made up of the thrust input δt and the control surface deflections of the rudder ζ , elevator η and aileron ξ

(2)
$$\underline{u} = \begin{bmatrix} \delta t & \xi & \eta & \zeta \end{bmatrix}^T.$$

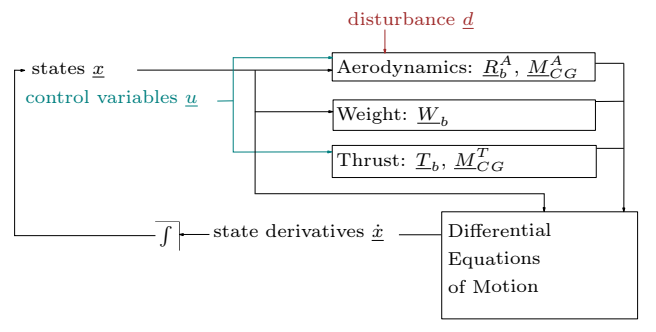


FIG 3. Complete flight mechanical model

Lastly, the wind velocity represents the only disturbance variable

$$\underline{d} = \underline{V}_w.$$

The weight force vector \underline{W}_b is modeled by assuming a constant mass. Further, a simple model is also used for the engine by assuming the transfer function from the control input δt , a pulse width modulated signal sent from the flight computer to the engine, to the thrust force, to be a simple gain. As the aircraft has a one-prop-on-the-nose configuration, the direction of the thrust force is aligned with the x-axis of the body frame and the thrust force is therefore only composed of an x-component. Moreover, in the postulated model of the Vitesse, the thrust does not cause a momentum around the center of gravity.

Besides the weight and the thrust forces, the aerodynamic forces and moments are acting on the AC. As this is the part of the model that will be improved through parameter estimation in this work, the modeling of the aerodynamics is of special interest. To avoid using computationally expensive methods like the potential theory, it is reasonable to use non-dimensional aerodynamic coefficients like C_L and C_m to display the dependencies of the acting forces on the incident flow. These coefficients can vary in the complexity of their composition depending on the objective and conditions. For this work, the aerodynamic coefficients include all derivatives listed in table 1. Each of these derivatives represents a partial derivative to a flight condition variable. Parameters that involve partial derivatives to other motion variables, for example

(4)
$$C_{Y\beta} = \frac{\partial C_Y}{\partial \beta},$$

are referred to as stability derivatives while derivatives with respect to control variables as for example

(5)
$$C_{Y\zeta} = \frac{\partial C_Y}{\partial \zeta}$$

are referred to as control derivatives. With all parameters listed in table 1, C_m for example is defined as

(6)
$$C_m = C_{m0} + C_{m\alpha} \cdot \alpha + C_{mq} \cdot \bar{q} + C_{m\eta} \cdot \eta.$$

L	ongitudi	nal		Lateral	
C_{D0}	C_{L0}	C_{m0}	C_{Y0}	C_{l0}	C_{n0}
C_{Dq}	$C_{L\alpha}$	$C_{m\alpha}$	$C_{Y\beta}$	$C_{l\beta}$	$C_{n\beta}$
$C_{D\eta}$	C_{Lq}	C_{mq}	C_{Yp}	$\overline{C_{lp}}$	C_{np}
$C_{D\alpha}$	$C_{L\eta}$	$C_{m\eta}$	C_{Yr}	C_{lr}	$\overline{C_{nr}}$
$C_{D\alpha^2}$	$C_{L\beta^2}$		$C_{Y\zeta}$	$C_{l\xi}$	$C_{n\xi}$
$C_{D\beta^2}$				$C_{l\zeta}$	$C_{n\zeta}$

Control Derivatives

Cross-Coupling between longitudinal and lateral

Cross-Coupling between roll and yaw

TAB 1. Aerodynamic Derivatives

Another classification that can be applied to the derivatives is the direction of action of the force or momentum that they are influencing. All parameters that describe an impact on the drag, lift or pitch are therefore listed under longitudinal, while those affecting the side force, the roll or yaw motion are lateral derivation. Those derivatives that portray an effect of a lateral flight parameter on a longitudinal force such as, for example, $C_{L\beta^2}$ are referred to as Cross-Coupling. However, Cross-Coupling effects can also be observed between roll and yaw motions as, for example, described by C_{np} .

The Vitesse V2 is a model motor glider of the manufacturer Dymond. Some dimensions of the aircraft are given in the manual [8] including the airfoil types and others were measured such as the airfoil coordinates of the stabilizers [9] and the mass of the fully equipped aircraft. To determine the tensor of inertia, the values of a similar aircraft model included in the open source model airplane simulator CRRCSim were used [9]. An overview of the dimensions can be found in 5.

The postulated flight mechanical model of the Vitesse V2 was developed by Wolfram Meyer-Brügel in 2015 and is a simplified flight dynamic simulation model based on the high precision flight simulator in [10]. The Simulink model that was also used in [9] draws data from two input files, a stability derivative file and a mass and inertia file that are results from a Vitesse model that was built in OpenVSP as described in [9]. As shown in figure 2 this flight mechanical model was used to incorporate into the filtering algorithm but also to generate log data to iteratively lay out the filter design. For the latter, sensor models with the specification obtained from the data sheets of the onboard sensors were added to the simulation. For the aircraft being considered, all the sensors used except the pitot probe and the GPS module are onboard the Pixhawk 4 mini flight computer. The angular rates as well as the accelerations are measured by the inertial measurement unit (IMU) BMI055. The height is determined using the barometric pressure measured by the MS5611 barometer, whereas the dynamic pressure is measured by the pitot probe equipped with the pres-

CC BY 4.0

sure transducer MS4525DO. In addition, the Neo-M8N GPS module is included to obtain the coordinates. An already implemented filter on the flight computer estimates the Euler angles from the measurements. Thus, the output vector of the system that is needed for the filtering algorithm can be defined as

$$(7) \quad \underline{y} = \begin{bmatrix} \underline{\omega}^T & \underline{\dot{V}}_{k_b}^T & \Phi & \Theta & \Psi & \underline{V}_{k_e}^T & h & p_{dyn} \end{bmatrix}^T.$$

3. KALMAN FILTERS

The structure of the Kalman filter as depicted in figure 4 is based on two steps: the prediction step or time update and the correction step or measurement update. In the prediction step, the predicted states and the predicted covariance matrix of the estimation error are determined. In the correction step, the output variables for the predicted states and given inputs, the Kalman gain, and the corrected states and covariances are determined. This basic structure underlies the classic Kalman filter as well as the EKF and the UKF.

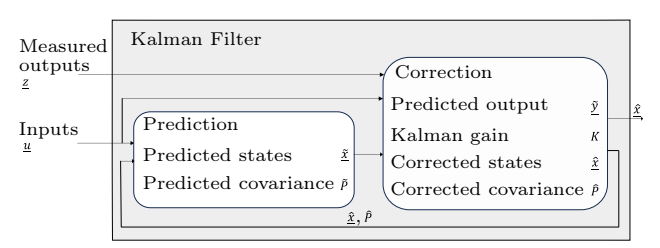


FIG 4. Kalman Filter structure

3.1. Extended Kalman Filter

While the original Kalman filter uses a linear model of a system to estimate the system's states, the EKF can be used for non-linear models. To estimate not only the states but also parameters such as stability and control derivatives, the state vector is augmented with the searched parameters. Subsequently, the non-linear filter is applied to the augmented states. The algorithm is described and explained in detail in [11].

3.2. Unscented Kalman Filter

For highly non-linear systems, even the EKF might decrease in performance. This is because the calculation of the covariance matrix includes the linearized version of the model. However, the more recently introduced UKF can show better performance using a method called the unscented transform [3]. A finite set of representative points, the so-called sigma points, that capture the mean and covariance of a probability distribution, is propagated through the nonlinear dynamics. The distribution of these points is specified by the scaling parameters α_{UKF} , β_{UKF} and κ . When designing the UKF, different cases that significantly affect the algorithm can be considered.

1. General case

Noise enters the system non-linearly. The augmented vector, therefore, has to be written as $\underline{x}_a = \begin{bmatrix} \underline{x}^T & \underline{\Theta}^T & \underline{w}^T & \underline{v}^T \end{bmatrix}^T.$

2. Special case

Additive zero-mean noise disturbances are assumed, and the augmentation of the state vector through the noise vector is not necessary. \underline{x}_a will then be composed as for the EKF: $\underline{x}_a = \begin{bmatrix} \underline{x}^T & \underline{\Theta}^T \end{bmatrix}^T$.

3.3. Filter Design

In order to implement the filters for the objective of parameter estimation in Matlab not only the algorithm, the modeled system and the definition of the parameters that will be estimated is necessary but also various design parameters have to be set.

For the EKF as well as for the UKF, the initial augmented states vector \underline{x}_{a0} , the initial covariance matrix P_{a0} , the process noise covariance Q and the measurement noise covariance R have to be set. Further, the scaling parameters α_{UKF} , κ , β_{UKF} have to be set for the UKF.

While the initial states \underline{x} can be set by taking the measurements or computed from the measured values, the initial values for the parameters that will be estimated $\underline{\Theta}$ are obtained from the aerodynamic model generated through VSPAERO. Regarding the covariance, the initial matrix represents the confidence in the starting values with a higher number indicating a lower confidence. As a first approach the diagonal terms of the matrix that represent the parameters are conservatively set to 10. However through an optimization process of the filters it was found that a lower initial covariance can improve the convergence of the parameters that are being estimated.

The process noise covariance matrix Q represents the system's noise and therefore also the uncertainties in the model of the system with a higher value indicating a higher uncertainty. Overall, if the matrix is set too small, the filter might not be able to track changes in the system dynamics which would result in poor performance. If Q is chosen too large, there is a risk that the filter will become unstable as a higher Q results in a bigger Kalman gain K. As an initial guess 10^{-5} is chosen and used for the optimization.

The measurement noise covariance matrix R is often seen as the counterpart to the process noise covariance Q. While Q indicates the trust in the model, R expresses how much the measurements can be trusted. Good estimations for the measurement noise covariance matrix R can be derived from the characteristics of the instrumentation used. The initial values for R derived from the specifications of the sensors listed in 2 can be found in [7]. To ensure the best outcome of the filters R was also optimized.

For the UKF the scaling parameters α_{UKF} , κ , β_{UKF} have to be set. The parameter α_{UKF} shall be between

CC BY 4.0

0.001 and 1 and determines the spread of the sigma points around x_a [12]. By varying κ the fourth and higher order moments of the sigma point distribution can be adjusted [5] and the parameter β_{UKF} can be used to include prior knowledge of the distribution of the states and parameters. For a Gaussian distribution setting β_{UKF} to 2 is optimal [12].

As it is shown in the visualization of the procedure of this work in figure 2, the design parameters of the filters were first tested using log data obtained through the simulation of the simulink model including the added sensor models and then optimized using the actual flight data. This optimization was performed by defining quality criteria of the parameter estimation outcome and using the global solver patternsearch() which is part of the MATLAB optimization toolbox. As quality criteria and cost function the relative standard deviation σ_{rel} of the parameters and the the normalized mean squared error (NMSE) are used. The relative standard deviation is computed through

(8)
$$\sigma_{rel} = \frac{100 \cdot \text{mean}_{100}(\sigma)}{|\text{mean}_{100}(\hat{x}_{param})|}$$

with σ being the standard deviation determined for every time step within the filtering algorithm through the square root of the updated covariance matrix as

(9)
$$\sigma = \sqrt{\hat{P}}.$$

 $mean_{100}(\sigma)$ in equation 8 therefore describes the mean of the standard deviations for the last 100 points. The NMSE is computed as

(10)
$$NMSE = \frac{\text{mean}((\tilde{y} - z)^2)}{\text{var}(z)}.$$

with mean($(\tilde{y}-z)^2$) being the mean of the squared residual meaning the difference between the estimated and the measured output and var(z) describing the variance of the measured outputs. For the mean as well as the variance the whole simulation except for the first 20 points is taken into account. This is because the filters need some time to follow the system's dynamics and especially for the purpose of parameter estimation the large residuals at the beginning of the simulation do not affect the relevant outcome.

The optimized filter parameters obtained through minimizing the mentioned quality criteria with the patternsearch() algorithm are listed in [7].

4. AERODYNAMIC PARAMETER IDENTIFICA-

In order to estimate the previously defined control and stability derivatives flight tests were prepared and conducted.

4.1. Flight tests

Prior to the conduct of flight tests, specific maneuvers were defined.

control input	objective
Elevator doublet	short period excitation
Elevator multistep	short period excitation
Elevator pulse	phugoid mode excitation
Aileron multistep	bank-to-bank maneuver
	roll mode excitation
Rudder doublet	Dutch Roll Excitation
Rudder pulses	achieving steady sideslip
Thrust variation	phugoid mode excitation

TAB 2. Flight maneuvers and control inputs

The selected maneuvers listed in table 2 all intend to excite different eigenmodes of the aircraft or achieve certain flight conditions that provide information about the longitudinal and lateral control and stability derivatives, as well as the cross-coupling effects. During the design process, all maneuvers are simulated using the Simulink model of the AC to ensure that the control inputs lead to the desired dynamic response.

By implementing the maneuvers on the Pixhawk 4 mini flight controller, the pressure on the pilot is minimized, and the exact execution of the control input is guaranteed.

The implementation is done in a way that allows the pilot to activate the maneuver as soon as the right flight conditions have been reached by flipping a switch. To activate the maneuver the aircraft has to be in stabilized mode. This mode which is already part of the PX4 Autopilot keeps the vehicle in a straight level flight position. As this is the initial position for all maneuvers, it is reasonable to start the control inputs from this mode. Further, it is possible to change the amplitude of the control input, as well as the Δt , the duration of a specific deflection, by changing different parameters in QGroundControl in the event that an eigenmode is not excited as expected.

4.1.1. Conduct of flight tests

5

The flight tests are conducted outside of Berlin on a day with very few clouds and wind velocities of around 4.7m/s. The software QGroundControl was used to track relevant quantities at all times and to change the before-explained parameters. The antenna connected to the computer running QGroundControl received telemetry data from the Holybro Telemetry Module that is operating at 433 MHz. Further, a FrSky Taranis Q X7 transmitter is used to communicate with the Pixhawk 4 mini and remotely control the Vitesse V2. Onboard the model motor glider,

a Ublox NEO-M8N GPS module, as well as the differential pressure sensor, MS4525DO, with a Pitot probe mounted on the right wing and a power module (PM02 V3) to measure voltage, current and power, are connected to the Pixhawk. As power supply, a Hacker LiPo battery (3s, 3800mAh) is integrated into the body of the plane, as shown in the schematic view in Figure 5.

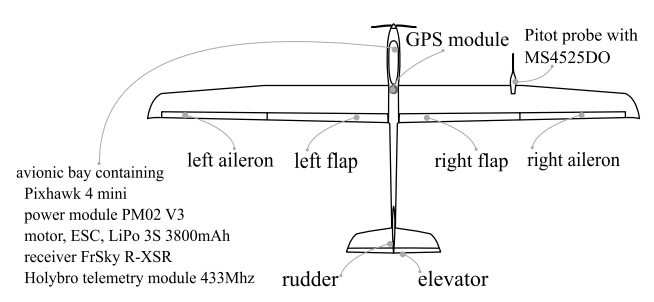


FIG 5. Schematic view of the Vitesse V2 [1]

In total, four flights were conducted. After the first one was an open loop flight that served to familiarize the pilot with the aircraft, in the second and third one maneuvers to characterize the longitudinal motion were executed. Lastly, during the fourth flight maneuvers affecting the lateral motion were carried out. Unfortunately, the destabilizing wind prevented the execution of the maneuvers that require a longer period of data acquisition such as the elevator pulse, the thrust variation and the rudder pulses.

4.2. Post-processing

The flight data was saved in a ULog file and processed using a MATLAB script. Relevant topics such as inputs (actuator outputs), measured outputs, and added parameters were extracted as time series, with most data logged at 100 Hz, except for GPS data limited to 5 Hz due to hardware constraints. To align the data on a common time axis, the time series were interpolated, and quaternions were converted to Euler angles. Control surface deflections were calculated from actuator PWM signals, and thrust was estimated using a proportional transfer function. An algorithm was implemented to save time series for each maneuver separately.

The maneuvers were then evaluated to identify those suitable for parameter identification.

After interpolating, saving, plotting and selecting suitable maneuvers, the data was used for the before mentioned optimization of the filter design parameters.

4.3. Results

With the optimized filters and the flight test data, the estimation of the aerodynamic derivatives listed in table 1 was pursued.

To estimate the derivatives of the longitudinal motion the parameters of the lateral motion were fixed on their initial values obtained from VSPAero. The Maneuver data of the 3-2-1-1 maneuver which is shown in figure

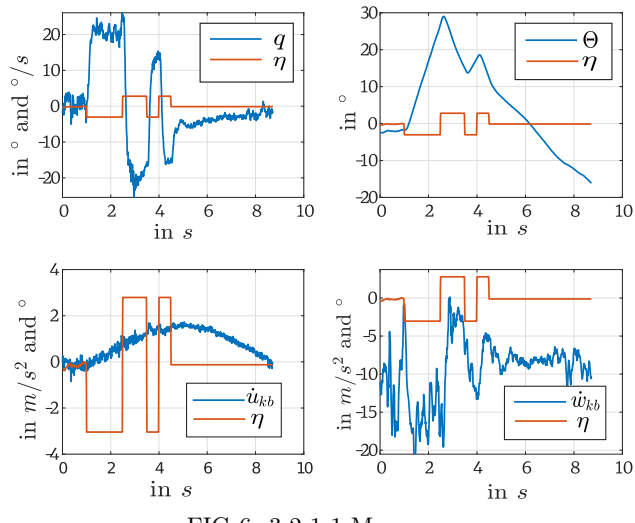


FIG 6. 3-2-1-1 Maneuver

6 is used as it is more informative than the elevator doublet due to the longer input and more changes. Further, the second before the maneuver is activated is also taken into account and the time series is concatenated four times as it increases the quality of the results.

Something that stands out in the plots of the aircraft's reaction to the elevator input is the smooth curve of the pitch angle which is due to the filtering of the Euler angles that is already implemented on the Pixhawk. Although the other measured quantities are noisy they show an overall expected behavior.

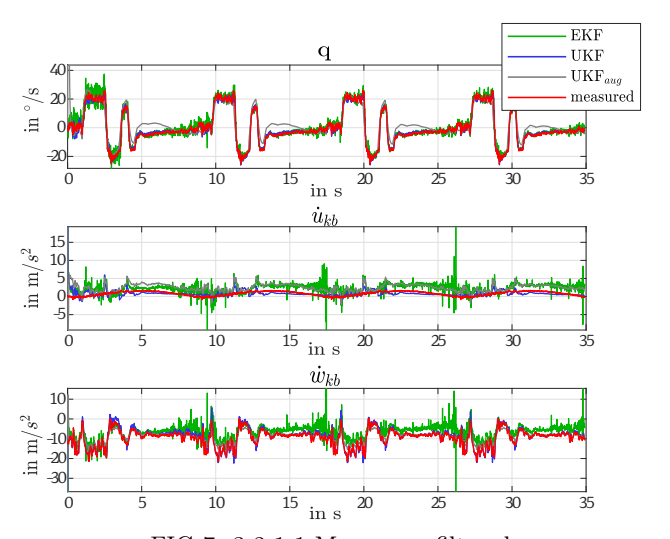


FIG 7. 3-2-1-1 Maneuver, filtered

Figure 7 shows the different filters' abilities to follow the system dynamics. As the pitch rate q is defined as a state, it includes the correction through the Kalman gain and is therefore estimated more accurately than the accelerations that are defined as outputs. A notable issue in all plots is the poor quality of the signals estimated by the Extended Kalman Filter (EKF). Although the pitch rate estimation becomes less noisy over time, it remains noisier than the measured signal by the end. During optimization, it was observed that reducing the measurement covariance, thus giv-

ing more weight to the measurements, can decrease the noise in the EKF estimation. However, this also results in reduced convergence of the estimated parameters, presenting a trade-off between signal noise reduction and parameter convergence.

Overall, figure 7 and the normalized mean squared error of all outputs listed in table 3 show that the UKF with additive zero mean noise is most capable to follow the system dynamics.

The resulting estimations of the aerodynamic parameters as well as their respective standard deviation and relative standard deviation is listed in table 6. More information including plots of the estimated parameters are portrayed in [7].

	EKF	UKF	$\mathrm{UKF}_{\mathrm{aug}}$
p	20	0.46	0.96
q	0.053	0.11	0.17
r	0.11	0.13	0.48
\dot{u}_{k_b}	10	1.4	9.4
\dot{v}_{k_b}	$2.3 \cdot 10^{+2}$	13	$1.3\cdot10^{+2}$
\dot{w}_{k_b}	1	0.072	0.24
Φ	9.2	0.017	3.5
Θ	9.7	0.41	7.9
Ψ	1.5	0.099	0.17
u_e	0.012	0.15	0.01
v_e	0.012	0.17	$7.9\cdot10^{-3}$
w_e	$3.6 \cdot 10^{-3}$	0.014	$1.7\cdot10^{-3}$
H	22	$7.8\cdot10^{-4}$	0.064
p_{dyn}	0.24	$5.8\cdot10^{-4}$	1.4

TAB 3. NMSE, 3-2-1-1 Maneuver

For the estimation of the lateral derivatives, the derivatives of the longitudinal motion are kept fixed at their initial values. However, it was not possible to filter the data multiple times by concatenating them as was done for the 3-2-1-1 maneuver. This is because the filter destabilized due to the jump in the values when going from the end of the maneuver to the beginning of it. The bank-to-bank maneuver and the rudder doublet were therefore filtered once.

Table 4 shows the normalized mean squared error for the outputs when using the bank-to-bank maneuver to estimate the lateral parameters. Similarly to the simulation of the 3-2-1-1 maneuver, the UKF shows the smallest errors for most of the outputs. The resulting parameter estimations are listed in 7. As for the outcome of the longitudinal parameter estimation some of the results seem realistic while many of them also show unlikely values or poor convergence. Since more data could have significantly improved the results, a much longer time period that does not include the predefined maneuvers and was flown by the pilot in open loop will be used for parameter estimation of the complete model.

The results generated through the simulation of the rudder doublet are described in [7] and do not provide any new significant findings.

	EKF	UKF	$\mathrm{UKF}_{\mathrm{aug}}$
p	11	1.5	1.7
q	25	11	96
r	2.6	2.6	0.81
u_{k_b}	$1.4 \cdot 10^{+2}$	7.7	50
v_{k_b}	$4.4 \cdot 10^{+2}$	$1.4\cdot10^{+2}$	29
$\dot{w_{k_b}}$	2.4	0.74	0.42
Φ	8.9	$4.3\cdot10^{-3}$	2.9
Θ	16	3.1	3.1
Ψ	19	1	15
u_e	0.22	0.052	0.088
v_e	0.051	$3.3\cdot10^{-3}$	$5.6\cdot10^{-3}$
w_e	0.028	$1.6\cdot10^{-3}$	$5.2\cdot10^{-4}$
H	10	$8.9\cdot10^{-5}$	0.031
p_{dyn}	1.5	$3.5\cdot10^{-4}$	2.4

TAB 4. NMSE, bank-to-bank Maneuver

Lastly, the flight data of the first flight which was flown in manual mode by the pilot was used for parameter identification of the complete model. During the flight, the pilot flew straight stretches of about 300 meters and executed turns with slight variations in altitude and velocity, while controlling the thrust, elevator, and aileron. The rudder deflection remained constant, preventing the estimation of rudder-related parameters. Additionally, the varying thrust, velocity, and altitude during the flight pose a challenge for parameter estimation, as aerodynamic derivatives, although assumed constant, are influenced by changing flight conditions [13].

While the parameters can be estimated together with the states, it is also possible to estimate only the parameters. To do so, we can treat the states as inputs and change the output vector to include the linear accelerations as well as the angular accelerations. Although linear accelerations are measured by the IMU, $\dot{\omega}$ should be derived from angular rate measurements. In general, this can be beneficial as it can decrease computational effort and increase the convergence of the parameters. However, treating the states as inputs also implies that we fully trust the measurements and do not take into account their measurement noise. While this might negatively impact the parameter estimation, the process will be evaluated based on the results and their quality criteria.

Furthermore, by treating the states as inputs the results of the UKF and UKF_{aug} will be closer together as the estimation of the system noise does not make a difference in their algorithms anymore. However, the estimation of measurement noise is still only part of the UKF_{aug}.

The table including the mean estimated parameters over the last 100 points as well as their standard deviations σ and σ_{rel} can be found in the appendix 8. Of the numerous aerodynamic coefficients, the lift and

CC BY 4.0

drag coefficients C_L and C_D play an important role. The results of the estimation of their derivatives are therefore depicted in figure 8 and 9.

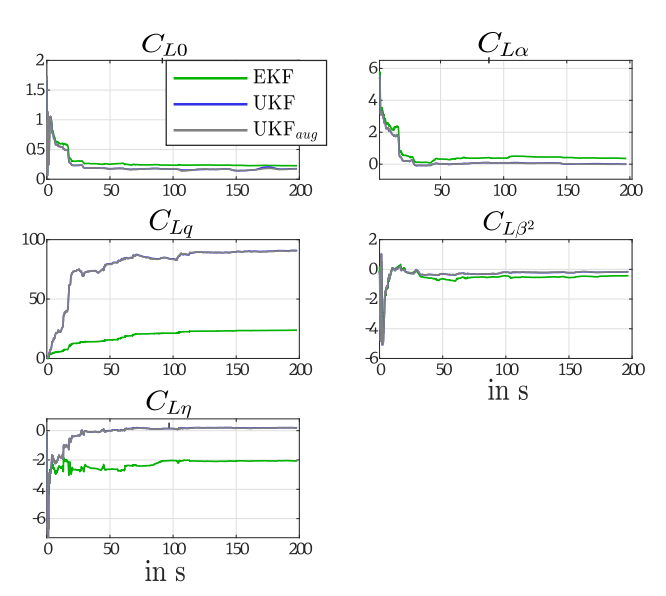


FIG 8. Lift derivatives, open loop flight

Overall, the results of the lift derivatives show good convergence for all filters. As expected, estimations by the UKF and UKF_{aug} are very close. To evaluate the plausibility of the results, the estimations are compared to the literature [13]. C_{L0} , $C_{L\eta}$ and $C_{L\beta^2}$ seem to show reasonable results except for the negative estimation of $C_{L\eta}$ by the EKF which does not appear plausible. Further, $C_{L\alpha}$ seems comparatively small and C_{Lq} is significantly too high. The reason for this might be model inaccuracies, as for example the assumption that the aerodynamic center and the center of gravity fall into the same position, which likely influences derivatives with respect to the pitch rate q. Additionally the assumption of no wind in the calculation of α and β together with the lack of measurement data of these quantities decreases the expected accuracy of the derivatives with respect to the aerodynamic

The outcome of the parameter estimation of drag derivatives as depicted in figure 9 shows parallels to the results for the lift derivatives. The plot of C_{Dq} indicates that the filters have difficulties estimating coefficients describing the effects of a change in the pitch rate. Again, this might be due to model inaccuracies. Furthermore, the overall convergence is significantly better than provided by the filtering of the maneuver data as it becomes evident when comparing the σ_{rel} in table 6 and 8.

While all drag derivatives seem plausible when compared to the literature those with respect to the aerodynamic angles, again, should be used with caution.

Similarly, the results of the pitch moment derivatives listed in table 8 seem overall realistic.

The lateral motion behaviour of the aircraft is described by the roll, side force and yaw derivatives

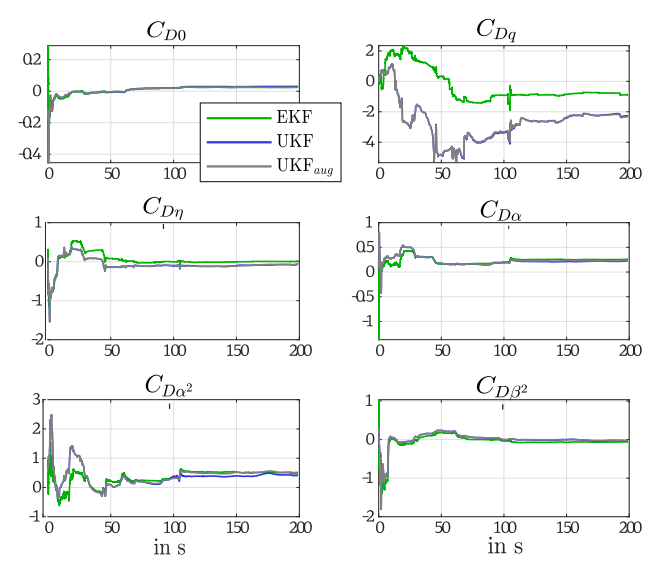


FIG 9. Drag derivatives, open loop flight

with their results listed in table 8. The derivative C_{l0} , C_{Y0} and C_{n0} describing the aircraft's behavior independent of all inputs and flight conditions are all close to zero indicating little asymmetric properties of the AC. Like this desired outcome most of the other derivatives show realistic and satisfactory results. All estimation plots can be found in [7].

Further, [7] shows that estimating both, parameters and states, from the same dataset also yielded mostly realistic results, though some outliers were noted, likely due to EKF instabilities and the complexity of the augmented UKF.

5. CONCLUSION

obtained data.

8

In order to identify the aerodynamic parameters of the Vitesse V2, a flight mechanical Simulink model of it was studied and transferred to MATLAB. Further, different Kalman Filter algorithms including the EKF, and two cases of the UKF were studied.

After implementing the model dynamics of the aircraft into the filter algorithms, the filters could be adjusted further through different parameters. In the first phase of the optimization the sensor data and the simulation output were used to improve the design parameters. By adding sensor models to the simulation model, a more realistic measurement output was created to verify the filter functionality. However, for a more effective optimization of the filters and eventually for parameter identification, real flight data was gathered in a flight test campaign with the Vitesse V2. Using previously defined quality criteria to evaluate the results of the filtering simulation,

To estimate the derivatives of the longitudinal motion, the maneuver data of a 3-2-1-1 elevator input was used. The UKF with additive zero-mean noise provided the most accurate tracking of system dynamics whereas the EKF showed more instability, making it harder to

the filter parameters were further optimized using the

balance reliance on measurements and the model. Despite noisy state estimates, the EKF's parameter convergence was satisfactory, similar to the UKF. However, all filters struggled with estimating C_{Lq} and C_{Dq} , possibly due to inaccuracies in the aerodynamic center and center of gravity. Unrealistic drag derivatives were likely caused by the lack of a thrust model, and assumptions of no wind impacted the estimation of the derivatives with respect to the aerodynamic angles α and β .

The data of a bank-to-bank maneuver and a rudder doublet that was used to estimate the derivatives of the lateral motion showed similar results concerning the better performance of the UKF in tracking the system dynamics.

Lastly, the full set of aerodynamic parameters but no states were estimated using manual flight data, showing more realistic results than in previous single-axis analyses, except for issues with C_{Lq} and aerodynamic angles. The larger dataset and simultaneous estimation of all parameters seemed to improve the overall parameter convergence as well as the concordance with comparative values from the literature. Despite potential uncertainties from height and velocity variations, the results were satisfactory.

Overall, all simulations show that the simplified UKF assuming additive zero-mean noise gives the best result regarding the ability to follow the system's dynamics as well as the convergence of the parameters and the concordance to comparative values. This superiority over the general case is possibly because the latter additionally tries to estimate the system and measurement noise with the same input data, allowing for more deviations.

Overall, the parameter identification results could be improved by adding information through measuring the aerodynamic angles α and β , for example using free movement vanes or a pressure based probe with two ports.

Moreover, the modeled aerodynamics could be more detailed. By determining the position of the aerodynamic center and by taking into account the lift acting on the tail and the lift acting on the wing and fuse-lage separately a more accurate structure of the model would enable a more precise parameter estimation.

When designing the maneuvers, the transfer function from the input signal to the control surface deflection or thrust force was estimated to be a simple gain. More accurate actuator models, however, could also increase the quality of the estimation outcome.

Lastly, for real time estimation and adaptive control the filter can be implemented on the pixhawk 4 mini flight computer on board the Vitesse.

Contact address:

mona.strauss@ipm.fraunhofer.de

References

- [1] Henrik Spark, Pedro González Ramirez, Christopher Ruwisch, Wolfram Meyer-Brügel, and Flávio J Silvestre. Development and experimental testing of flight path control using total energy control and siso control loops. In AIAA SCITECH 2023 Forum, page 0104, 2023.
- [2] Rudolph E Kalman and Richard S Bucy. New results in linear filtering and prediction theory. Journal of Basic Engineering, pages 95–108, 1961.
- [3] Simon J Julier and Jeffrey K Uhlmann. New extension of the kalman filter to nonlinear systems. 3068:182–193, 1997.
- [4] Reiner Marchthaler and Sebastian Dingler. Kalman-Filter. Springer, 2017. ISBN: 978-3-658-16728-8.
- [5] Simon Julier, Jeffrey Uhlmann, and Hugh F Durrant-Whyte. A new method for the nonlinear transformation of means and covariances in filters and estimators. IEEE Transactions on automatic control, 45(3):477–482, 2000.
- [6] Hans Wilhelm Knobloch and Huibert Kwakernaak. Der optimale beobachter. optimale ausgangsregelung. Lineare Kontrolltheorie, pages 235–258, 1985.
- [7] Mona Strauss. Master Thesis: Parameter Identification via Kalman Filter on a model motor glider. 2023.
- [8] Gustav Staufenbiel GmbH. Dymond modell-sport anleitung vitesse v2, March 13th 2012. https://www.horizonhobby.de/on/demandware.static/Sites-horizon-eu-Site/Sites-horizon-master/default/Manuals/HSF0314063EV2-Manual-DE.pdf.
- [9] Henrik Spark. An assessment of aircraft control via siso control loops and total energy control. Deutscher Luft- und Raumfahrtkongress 2021, 2021.
- [10] Wolfram Meyer-Brügel. Präzisere Echtzeit-Flugsimulation kleiner Nutzflugzeuge durch Integration feingranularer Teilmodelle: am Beispiel der Aktuator- und Fahrwerksmodellierung. TU Berlin, 2019.
- [11] Ravindra V. Jategaonkar. Flight Vehicle System Identification: A Time-Domain Methodology Second Edition. American Institute of Aeronautics and Astronautics, 2015.
- [12] Eric A Wan and Rudolph Van Der Merwe. The unscented kalman filter for nonlinear estimation. In Proceedings of the IEEE 2000 Adaptive Systems for Signal Processing, Communications, and Control Symposium (Cat. No. 00EX373), pages 153–158. Ieee, 2000.
- [13] Rudolf Brockhaus. Flugregelung. Springer-Verlag, 2013.

CC BY 4.0

A. APPENDIX

A.1. Dimensions of Vitesse V2

physical quantity	symbol	value
tensor of inertia	J	$\begin{bmatrix} 0.9006 & 0 & 0 \\ 0 & 0.2487 & 0 \\ 0 & 0 & 1.1469 \end{bmatrix} \text{ kg m}^{-2}$
wing surface	S	0.61681 m^2
wing span	b	2.9690 m
aerodynamic chord length	l_{MAC}	$0.1673~\mathrm{m}$
mass	m	3.1 kg

TAB 5. Dimensions of the Vitesse V2

A.2. Simulation Results

A.2.1. 3-2-1-1 Maneuver

	EKF				UKF			$\mathrm{UKF}_{\mathrm{aug}}$		
	mean	σ	σ_{rel}	mean	σ	σ_{rel}	mean	σ	σ_{rel}	
C_{m0}	0.52	0.038	7.2	-0.035	$9.7\cdot10^{-3}$	28	-0.67	$7.5\cdot10^{-3}$	1.1	
$C_{m\alpha}$	-1.1	0.083	7.7	-0.83	0.066	8	1.2	0.013	1.1	
C_{mq}	-14	0.1	0.73	-14	0.1	0.74	-18	0.09	0.49	
$C_{m\eta}$	-1.1	0.097	9.1	-1.1	0.096	8.4	-0.98	$9.4\cdot10^{-3}$	0.96	
C_{D0}	0.71	$1.5\cdot 10^{-3}$	0.22	$-1.4 \cdot 10^{-3}$	$5.1\cdot10^{-4}$	36	-1.5	0.02	1.3	
C_{Dq}	1.4	0.026	1.8	3.7	0.089	2.4	7.8	0.067	0.86	
$C_{D\eta}$	-0.7	$5.2\cdot10^{-3}$	0.74	-0.32	0.01	3.1	0.046	$7.2\cdot10^{-3}$	15	
$C_{D\alpha}$	-2.4	$6.2\cdot10^{-3}$	0.26	-0.025	$3.3\cdot10^{-3}$	13	4.5	0.063	1.4	
$C_{D\alpha^2}$	2.1	$7.9\cdot10^{-3}$	0.38	0.09	$9.5\cdot10^{-3}$	11	-2.7	0.051	1.9	
C_{L0}	-4.1	$8.4\cdot10^{-3}$	0.2	0.38	$3.8\cdot10^{-3}$	1	-8	0.027	0.34	
$C_{L\alpha}$	11	0.016	0.15	2.7	0.025	0.94	16	0.047	0.3	
$C_{L\beta^2}$	-2.8	0.014	0.49	-1.5	0.047	3.3	-3.2	0.033	1	
$C_{L\eta}$	0.19	0.033	18	0.75	0.063	8.4	1.8	0.039	2.1	

TAB 6. Aerodynamic Derivatives Results for 3-2-1-1 Maneuver

A.2.2. Bank to bank Maneuver

	EKF			UKF			$\mathrm{UKF}_{\mathrm{aug}}$		
	mean	σ	σ_{rel}	mean	σ	σ_{rel}	mean	σ	σ_{rel}
C_{l0}	0.13	0.026	19	-0.1	$9.6\cdot10^{-3}$	9.5	-5.6	0.019	0.33
C_{leta}	0.19	0.052	28	0.78	0.067	8.6	16	0.035	0.22
C_{lp}	-1.5	0.086	5.7	-0.029	0.085	300	2.8	0.013	0.48
C_{lr}	-0.7	0.096	14	-0.21	0.096	45	-4.8	0.033	0.69
$C_{l\xi}$	-1	0.088	8.4	0.068	0.088	130	0.36	0.045	13
C_{n0}	-0.16	0.015	9.1	0.17	$6.3\cdot10^{-3}$	3.6	-0.72	$3.2\cdot10^{-3}$	0.44
$C_{n\beta}$	0.12	0.029	24	-0.99	0.044	4.4	2	$6.6\cdot10^{-3}$	0.33
C_{np}	-0.43	0.063	15	-1.8	0.064	3.5	0.54	$2.6\cdot10^{-3}$	0.48
C_{nr}	0.78	0.091	12	0.62	0.089	14	-1.2	$9.6\cdot10^{-3}$	0.78
$C_{n\xi}$	0.94	0.068	7.2	-1.1	0.068	6.2	0.36	$8.7\cdot10^{-3}$	2.4
C_{Y0}	-0.042	$4.4\cdot10^{-3}$	11	0.063	$1.4\cdot10^{-3}$	2.2	0.27	$7.2\cdot10^{-3}$	2.7
$C_{Y\beta}$	0.013	$8.8 \cdot 10^{-3}$	68	-0.56	0.011	1.9	-0.95	0.013	1.4
C_{Yp}	1.8	0.01	0.57	1.6	0.023	1.4	-4.5	0.011	0.24
C_{Yr}	-0.23	0.028	12	0.4	0.036	9.2	-6.7	0.036	0.54

TAB 7. Aerodynamic Derivatives Results for bank-to-bank Maneuver

A.2.3. Open-loop flight

	EKF				UKF		$\mathrm{UKF}_{\mathrm{aug}}$		
	mean	σ	σ_{rel}	mean	σ	σ_{rel}	mean	σ	σ_{rel}
C_{l0}	$4.1\cdot10^{-3}$	$1.0 \cdot 10^{-4}$	2.4	$4.7 \cdot 10^{-3}$	$9.9\cdot10^{-5}$	2.1	0.01	$1.3\cdot 10^{-4}$	1.2
$C_{l\beta}$	$-4.4\cdot10^{-4}$	$2.4\cdot10^{-4}$	55	$-8.6 \cdot 10^{-3}$	$1.4\cdot10^{-4}$	1.6	-0.032	$1.5\cdot 10^{-4}$	0.48
C_{lp}	-0.07	$2.2\cdot 10^{-3}$	3.2	-0.064	$2.2\cdot10^{-3}$	3.5	-0.065	$2.2\cdot 10^{-3}$	3.5
C_{lr}	0.039	$2.2\cdot 10^{-3}$	5.6	0.034	$2.0\cdot10^{-3}$	6	0.08	$2.2\cdot10^{-3}$	2.7
$C_{l\xi}$	-0.096	$2.1\cdot10^{-3}$	2.2	-0.083	$2.1\cdot10^{-3}$	2.6	-0.093	$2.1\cdot10^{-3}$	2.3
C_{m0}	$2.5\cdot10^{-3}$	$1.7\cdot10^{-4}$	6.9	$-1.9 \cdot 10^{-3}$	$1.7\cdot10^{-4}$	9.1	$-3.5 \cdot 10^{-3}$	$1.8\cdot10^{-4}$	5.2
$C_{m\alpha}$	0.011	$1.4\cdot10^{-3}$	13	$-5.2\cdot10^{-3}$	$1.4\cdot10^{-3}$	27	0.02	$1.4\cdot10^{-3}$	7.2
C_{mq}	-9.5	0.069	0.72	-9.1	0.073	0.81	-8.6	0.073	0.85
$C_{m\eta}$	-0.51	$4.3\cdot10^{-3}$	0.84	-0.5	$4.5\cdot10^{-3}$	0.9	-0.47	$4.5\cdot10^{-3}$	0.97
C_{n0}	$3.8\cdot10^{-3}$	$4.9\cdot10^{-5}$	1.3	$3.6 \cdot 10^{-3}$	$4.9\cdot10^{-5}$	1.4	$3.9 \cdot 10^{-3}$	$4.9\cdot10^{-5}$	1.3
$C_{n\beta}$	$1.4\cdot10^{-3}$	$1.1\cdot 10^{-4}$	8.2	$1.5 \cdot 10^{-3}$	$1.2\cdot 10^{-4}$	7.9	$4.1 \cdot 10^{-4}$	$1.1\cdot 10^{-4}$	28
C_{np}	$-9.7\cdot10^{-3}$	$1.1\cdot10^{-3}$	11	-0.021	$1.1\cdot10^{-3}$	5.2	-0.022	$1.1\cdot10^{-3}$	4.8
C_{nr}	$-5.6\cdot10^{-3}$	$1.0\cdot10^{-3}$	19	-0.025	$1.0\cdot10^{-3}$	4.2	-0.021	$1.0\cdot10^{-3}$	5.1
$C_{n\xi}$	$5.8\cdot10^{-3}$	$1.0\cdot10^{-3}$	18	$5.5 \cdot 10^{-3}$	$1.0\cdot10^{-3}$	19	$-1.8 \cdot 10^{-3}$	$1.0\cdot10^{-3}$	57
C_{D0}	0.031	$7.5\cdot10^{-5}$	0.24	0.027	$8.6\cdot10^{-5}$	0.32	0.024	$8.9\cdot10^{-5}$	0.36
C_{Dq}	-0.88	0.011	1.3	-2.3	0.029	1.3	-2.3	0.029	1.2
$C_{D\eta}$	0.017	$1.1\cdot10^{-3}$	6.3	-0.069	$1.4\cdot10^{-3}$	2.1	-0.056	$1.4\cdot10^{-3}$	2.6
$C_{D\alpha}$	0.26	$4.7 \cdot 10^{-4}$	0.18	0.23	$5.4 \cdot 10^{-4}$	0.24	0.24	$5.2\cdot10^{-4}$	0.22
$C_{D\alpha^2}$	0.47	$2.1\cdot10^{-3}$	0.45	0.41	$2.2\cdot10^{-3}$	0.54	0.52	$2.3\cdot 10^{-3}$	0.45
$C_{D\beta^2}$	-0.064	$8.0\cdot10^{-4}$	1.2	-0.034	$8.2\cdot10^{-4}$	2.4	-0.027	$8.1\cdot10^{-4}$	3
C_{Y0}	$-8.5\cdot10^{-3}$	$6.9\cdot10^{-5}$	0.81	-0.011	$7.1\cdot10^{-5}$	0.64	-0.01	$7.0\cdot10^{-5}$	0.67
$C_{Y\beta}$	$8.8\cdot10^{-3}$	$2.6\cdot10^{-4}$	3	0.016	$2.7\cdot10^{-4}$	1.6	0.015	$2.7\cdot 10^{-4}$	1.8
C_{Yp}	0.3	$1.5\cdot 10^{-3}$	0.5	0.33	$1.5\cdot 10^{-3}$	0.44	0.18	$1.5\cdot 10^{-3}$	0.81
C_{Yr}	2.8	$2.3\cdot10^{-3}$	0.079	2.9	$2.4\cdot10^{-3}$	0.082	2.6	$2.4 \cdot 10^{-3}$	0.091
C_{L0}	0.22	$5.1\cdot10^{-5}$	0.023	0.18	$6.7\cdot10^{-5}$	0.037	0.18	$1.1\cdot10^{-4}$	0.06
$C_{L\alpha}$	0.34	$2.6\cdot10^{-4}$	0.077	$4.2 \cdot 10^{-4}$	$2.8\cdot10^{-4}$	66	-0.014	$2.8\cdot 10^{-4}$	2
C_{Lq}	24	$3.6\cdot10^{-3}$	0.015	91	0.023	0.025	90	0.022	0.025
$C_{L\beta^2}$	-0.42	$5.1\cdot10^{-4}$	0.12	-0.16	$5.4\cdot10^{-4}$	0.33	-0.18	$5.4\cdot10^{-4}$	0.3
$C_{L\eta}$	-2.1	$7.4\cdot10^{-4}$	0.036	0.19	$9.9\cdot10^{-4}$	0.52	0.18	$9.8\cdot10^{-4}$	0.54

TAB 8. Aerodynamic Derivatives Results for open loop flight, only parameters estimated